Supporting information

Visible Surface Plasmon Modes in Single Bi_2Te_3 Nanoplate

Meng Zhao,[†, ‡] *Michel Bosman,*[§] *Mohammad Danesh,*[//,#] *Minggang Zeng,*[‡, ▽] *Peng Song,*[†,‡]

Yudi Darma,[⊥, ▽] *Andrivo Rusydi,*[⊥, ▽] *Hsin Lin,*[‡, ▽] *Cheng-Wei Qiu,*[//] *and Kian Ping Loh*[†,‡,*]

[†]Department of Chemistry, National University of Singapore, 3 Science Drive 3, 117543, Singapore

[‡]Centre for Advanced 2D Materials and Graphene Research Centre, National University of Singapore, 6 Science Drive 2, 117546, Singapore

[§]Institute of Materials Research and Engineering, A*STAR (Agency for Science, Technology and Research), 2 Fusionopolis Way, 138634, Singapore

[//]Department of Electrical and Computer Engineering, National University of Singapore, 4 Engineering Drive 3, 117583, Singapore

[#]Electronics and Photonics Department, Institute of High Performance Computing, 1 Fusionopolis Way, Singapore 138632

[▽]Department of Physics, National University of Singapore, 2 Science Drive 3, 117542, Singapore

[⊥]Singapore Synchrotron Light Source, National University of Singapore, 117603, Singapore

[*]E-mail: chmlohkp@nus.edu.sg

Experimental details

Synthesis and characterisations of Bi_2Te_3 nanoplates. Bi_2Te_3 nanoplates were synthesised by the solvothermal method. In a typical process, polyvinylpyrrolidone (0.3 g), Bi_2O_3 (0.5 mmol), TeO_2 (1.5 mmol) and 2 mL of NaOH solution (5 mol/L) were added in ethylene glycol (18 mL). The resulting suspension was transferred to an autoclave and kept at 210 ℃ for 4 h. After cooling to room temperature, the synthesised products were collected by centrifugation and washed several times with distilled water, absolute ethanol and isopropyl alcohol. The nanoplates were characterized with SEM, TEM, XRD and AFM.

EELS and CL. Bi_2Te_3 nanoplates were drop-casted onto a 30 nm thick silicon nitride membrane and then annealed under Ar/H_2 atmosphere to remove impurities and the oxidised layer. The EELS measurements were carried out using an FEI Titan TEM equipped with a Schottky electron source in STEM mode. STEM was operated at 80 kV for all measurements. A convergence semiangle of 13 mrad was used and the electron beam was focused to a diameter of approximately 1 nm. A Wien-type monochromator was used to disperse the electron beam in energy, from which a monochrome electron beam was formed using a narrow energy-selecting slit. This resulted in an energy resolution of 70 meV as full-width at half-maximum (FWHM) value. A Gatan Tridiem ER EELS detector was used for EELS mapping and spectroscopy, using a collection semiangle of 12 mrad. Spectra were collected using the binned gain averaging method. EELS maps were obtained by scanning a rectangular raster of pixels with the 1 nm electron probe and mapping the EELS counts in each pixel using an energy window of 0.1 eV. CL was performed in the same FEI Titan TEM about 20 times more current in the ~1 nm electron probe, this time without the monochromator excited.. All CL spectra were acquired in 60 s using a Gatan Vulan cathodoluminescence detector.

Spectroscopic ellipsometry. A Bi_2Te_3 film was prepared on single-side-polished quartz for ellipsometry measurements, which were taken using a Sentech SE850 ellipsometer equipped with light sources ranging from 0.5 eV to 6.3 eV. Data for □ (amplitude ratio) and Δ (phase difference) between the p- and s- polarised light waves were taken with an incident angle of 80^{o}. To extract the dielectric function of Bi_2Te_3, multilayer modelling was performed, taking into account reflections at each interface through Fresnel coefficients[1].

EELS simulations. The simulations were carried out with the infinite element method using COMSOL. A hexagonal Bi_2Te_3 crystal with a thickness of 10 nm was modelled on top of a 30 nm thick Si_3N_4. Experimental complex permittivity values were used and the refractive index of the substrate was taken from the literature[2]. An electron beam with a radius of 0.5 nm impinged upon the centre and edge (2 nm away) of the crystal. The mesh in the transverse plane was triangular with elements as small as 0.1 nm at the beam position and at edges. The mesh was non-uniformly swept along the direction of beam propagation. To accurately take into consideration the abrupt changes created in the normal electric field component at the interfaces, the mesh size was 0.1 nm at the crystal/substrate/air interfaces. MNPBEM toolbox based on the boundary element method was used to calculate EELS maps[3]. The current distribution was calculated using a plasmonic quasistatic eigenvalue mode solver.

An electron moving with a velocity vector v with uniform speed can be modeled with a charge density and current density of the q-w space as[4]

$$\mathbf{j}(\mathbf{r}, \omega) = -e\delta(x - x_0)\delta(y - y_0)e^{iqz}\hat{a}_z$$

Considering the cylindrical symmetry of structure the potentials can be written using Bessel functions as[3]

$$\phi = -\frac{2}{v_e\, \epsilon_r} K_0\left(\frac{qR}{\gamma}\right) e^{iq(z-z_0)}$$

$$A = \hat{\mathbf{z}}\epsilon_r \frac{v_e}{c}\phi$$

And the radiated electromagnetic fields can be calculated as:

$$E = ikA - \nabla\Phi$$

$$\mathbf{E}(\mathbf{r},\omega) = \frac{2e\omega}{v_e^2\gamma\,\epsilon_r} e^{iq(z-z_0)}[\frac{i}{\gamma}K_0\left(\frac{qR}{\gamma}\right)\mathbf{z} - K_1\left(\frac{qR}{\gamma}\right)(\cos\phi\,\mathbf{x} + \sin\phi\,\mathbf{y})]$$

$$\gamma = \left(1 - \epsilon_r\frac{v_e^2}{c^2}\right)^{-1/2}$$

$$q = \omega/v_e$$

The radiated electromagnetic field can be used to calculate the scattered electromagnetic fields under the scattering field formalism. A full wave calculation of the scattered fields is performed with the finite element method using the commercial software COMSOL. In order to calculate the EELS loss probability, the work done on the electron along its propagation direction is calculated by integrating the following equation along the propagation direction[4]

$$\Gamma_{EELS} = \frac{e}{\pi\omega\hbar}\int Re\left\{e^{-i\omega t}\,\mathbf{V}\cdot\mathbf{E}(\boldsymbol{r}(t),\omega)\right\}dt$$

The surface charge density is plotted by applying the boundary conditions 0.1nm above and below the surface of the crystal and calculating the difference in the normal electric field component:

$$(\mathbf{D_2} - \mathbf{D_1})\cdot\hat{\mathbf{n}}_{12} = \rho_s$$

DFT calculation. The calculations of the electronic properties of Bi_2Te_3 slab were performed using density functional theory in the Vienna *ab initio* Simulation Package[5]. The generalisedgradient approximation (GGA) of Perdew, Burke, and Ernzerhof (PBE) for exchange and correlation (XC) was adopted[6]. The Bi_2Te_3 slab consisted of 12 quintuple layers and a vacuum layer of 15 Å, which is sufficient to avoid the artificial interaction between the periodic images of Bi_2Te_3 films. A 7 ×7 Γ-centred grid was used to sample the Brillion zone. Wave functions were generated by the projector-augmented wave method with energy cut-off of 200 eV. The SOC was taken into account as a second variational step using eigen functions from scalar relativistic calculations. With the converged electronic ground state and the independent-quasiparticle approximation[7], the frequency-dependent, complex dielectric function of Bi_2Te_3 slab was calculated with 200 energy grid points and 312 empty conduction bands.

Supporting Figures

Control of nanoplate Size. The size of Bi_2Te_3 nanoplates can be controlled by using different reducing agents. Supplementary Figure 1 shows that the size of synthesized nanoplate decreases with the use of a stronger reducing agent. By using reducing agents of 15% IPA + 85% EG, EG, 50% EG +50% glycerol, glycerol, Bi_2Te_3 nanoplates with average edge-to-edge distance of 1 µm, 700 nm, 300 nm, 150 nm were obtained, respectively.

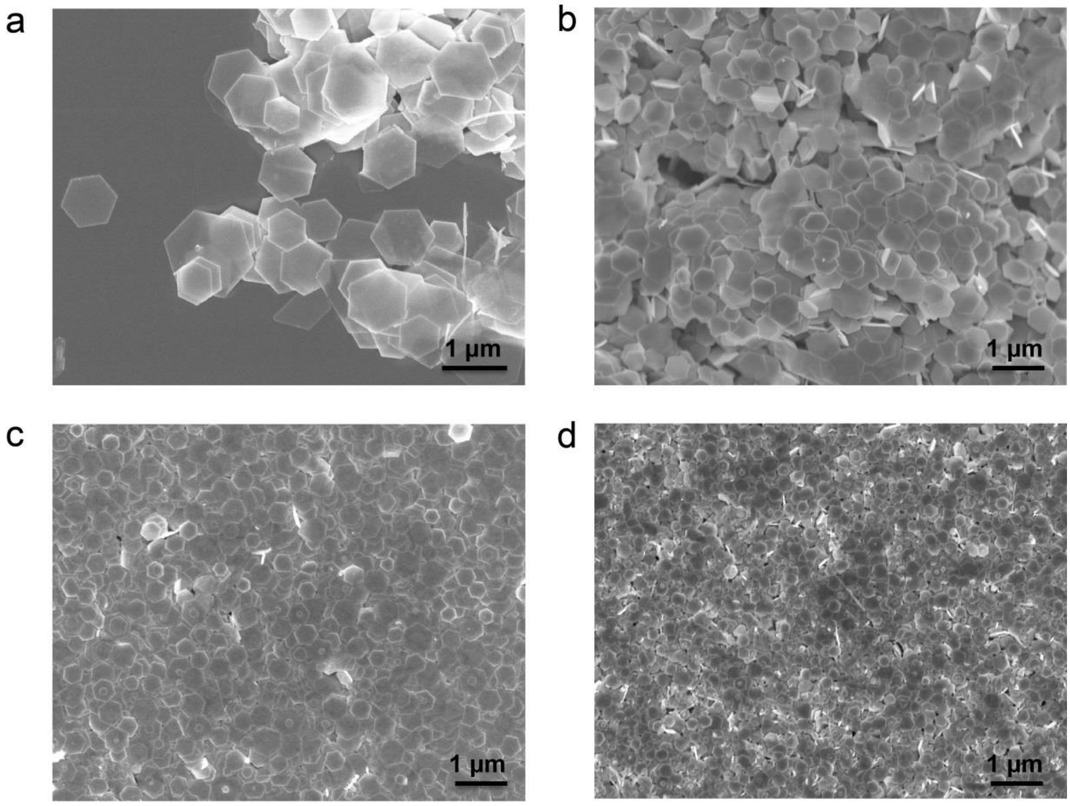

Figure S1. SEM images of Bi_2Te_3 nanoplates with average edge-to-edge distance of (a) 1 µm (b)700 nm (c) 300 nm (d) 150 nm.

Height profiles of nanoplates. Figure S2 shows a typical AFM image and corresponding height profiles. The nanoplates show well defined hexagonal shape with atomic flat surface and thickness of 10-16 nm.

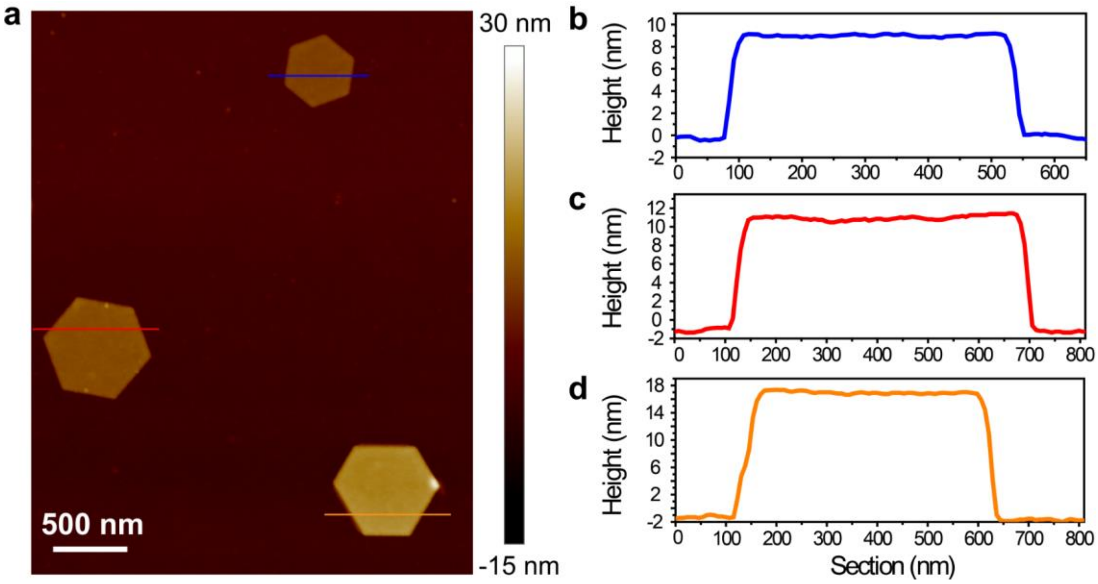

Figure S2. (a) Topographical AFM image of three Bi_2Te_3 nanoplates. (b) Corresponding height profiles of the top nanoplate shown in (a) with thickness of 9 nm. (c) Corresponding height profiles of the middle nanoplate shown in (a) with thickness of 12 nm. (d) Corresponding height profiles of the bottom nanoplate shown in (a) with thickness of 18 nm.

Bulk UV-Vis absorption. Figure S3 shows a board absorption, which represents the overall plasmonic effects of Bi_2Te_3 nanoplates ensemble. The UV-Vis absorption agrees well with the TEM-EELS results, despite a little shift of the peaks due to the fact that TEM-EELS measurements were carried on individual nanoplates while UV-Vis absorption measured the bulk solution. Light harvesting in the visible range can be significantly improved, suggesting that Bi_2Te_3 nanoplates show good promise in solar energy utilization.

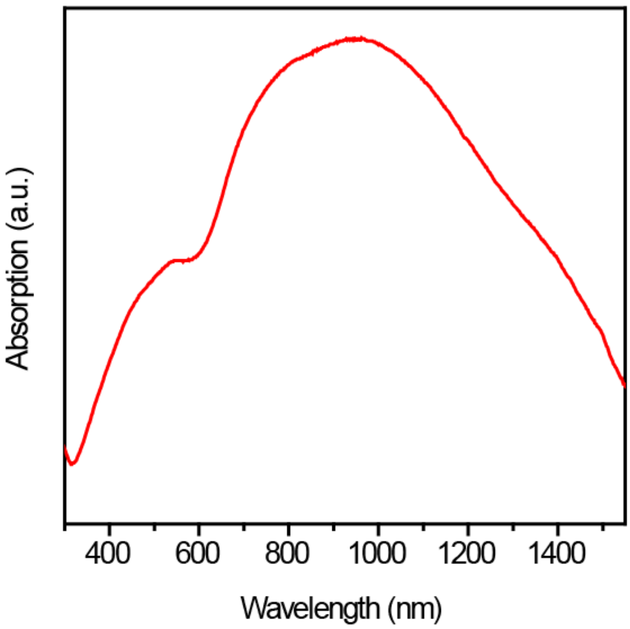

Figure S3. UV-Vis absorption spectrum of Bi_2Te_3 nanoplates dispersed in isopropyl alcohol.

Size dependent EELS. Bi_2Te_3 nanoplates with edge-to-edge distance of 150, 300 and 700 nm were identified under STEM and the corresponding EEL spectra were collected. Figure S4 shows that the edge mode and center modes exhibit similar size dependence, i.e. the plasmon energies decrease with the increase of nanoplate size.

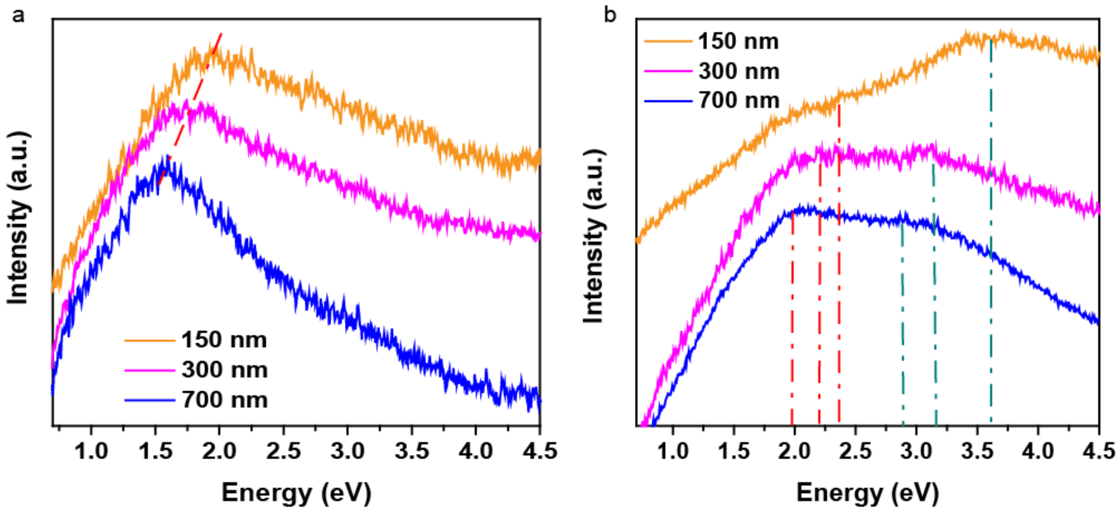

Figure S4. Edge mode (a) and center mode (b) EEL spectra of three hexagonal nanoplate with edge-to-edge distance of 150, 300, 700 nm. The largest one is the same as the one studied in the main text.

Thickness dependent dielectric function. Figure S5 shows that the dielectric function and energy loss function are independent of the thickness of Bi_2Te_3. By changing the thickness from 6 QL to 12 QL, the zero-cross frequency of ε_1 and peaks position of energy loss function remain unchanged. This indicates that these features are dominated by surface states of Bi_2Te_3 and the contributions of bulk states are not significant.

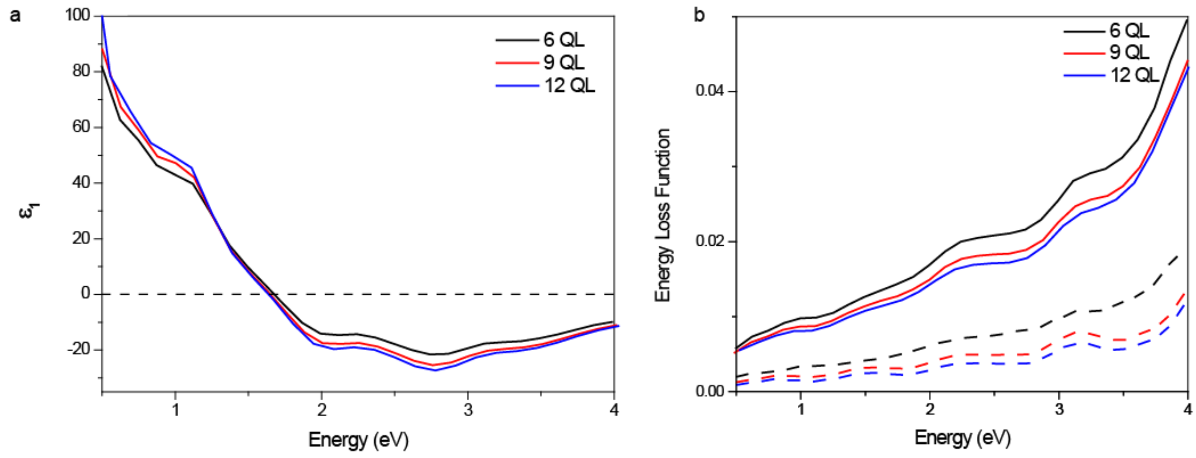

Figure S5. Calculated (a) dielectric function and (b) energy loss function (solid lines) and corresponding surface contributions (dashed lines) of Bi_2Te_3 slab with 6, 9 and 12 QL.

SOC effect. Figure S6 shows the calculated band structure, dielectric function and ELF of a 12QL Bi_2Te_3 slab without SOC effect. A band gap of 0.33 eV exists in the absence of the SOC effect and the dielectric function deviates from the experimental spectra substantially. Regarding the ELF, the peaks at 2.1 eV and 3.1 eV vanish in the absence of SOC effects.

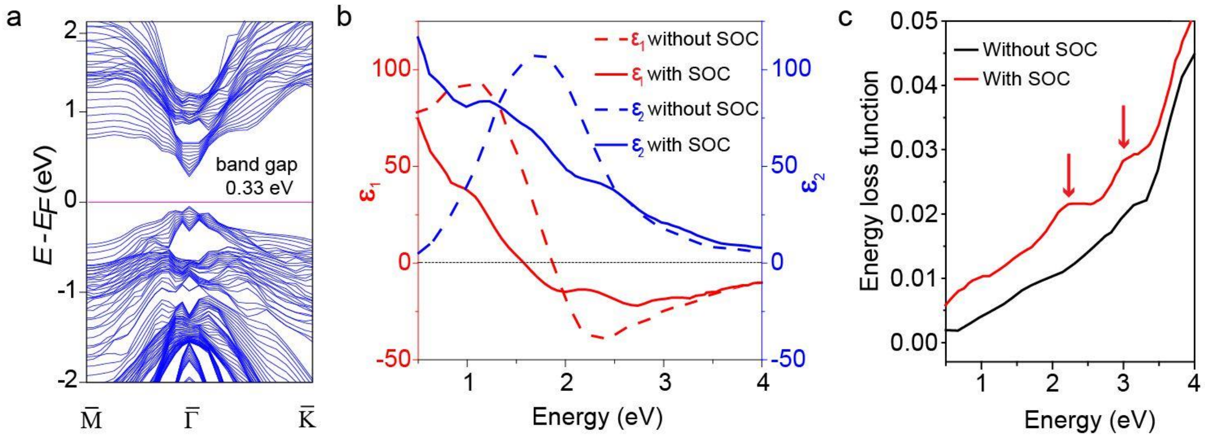

Figure S6. (a) Band structure of a 12QL Bi_2Te_3 slab without SOC effect. (b) Dielectric function and (c) ELF of the same Bi_2Te_3 slab with and without SOC effect.

References

(1) Fujiwara, H., *Data Analysis In Spectroscopic Ellipsometry*, John Wiley & Sons, Ltd, 2007, 147-207.

(2) Philipp, H. R. *J. Electrochem. Soc.* **1973,** 120, (2), 295-300.

(3) Hohenester, U. *Comput. Phys. Commun.* **2014,** 185, (3), 1177-1187.

(4) de Abajo, F. J. G.; Kociak, M. *Phys. Rev. Lett.* **2008,** 100, (10), 106804.

(5) Kresse, G.; Hafner, J. *Phys. Rev. B* **1993,** 47, (1), 558-561.

(6) Perdew, J. P.; Burke, K.; Ernzerhof, M. *Phys. Rev. Lett.* **1996,** 77, (18), 3865-3868.

(7) Gajdoš, M.; Hummer, K.; Kresse, G.; Furthmüller, J.; Bechstedt, F. *Phys. Rev. B* **2006,** 73, (4), 045112.